Light extraction from surface plasmons and waveguide modes in an organic light-emitting layer by nanoimprinted gratings

Jörg Frischeisen,[1,*] Quan Niu,[2] Alaa Abdellah,[2] Jörg B. Kinzel,[1] Robert Gehlhaar,[3] Giuseppe Scarpa,[2] Chihaya Adachi,[3,4] Paolo Lugli,[2] and Wolfgang Brütting[1,5]

[1] *Institute of Physics, University of Augsburg, Universitätsstrasse 1, 86159 Augsburg, Germany*
[2] *Institute for Nanoelectronics, Technische Universität München, Arcisstrasse 21, 80333 Munich, Germany*
[3] *Center for Future Chemistry, Kyushu University, 744 Motooka, Nishi, Fukuoka 819-0395, Japan*
[4] *Center for Organic Photonics and Electronics Research (OPERA), Kyushu University, 744 Motooka, Nishi, Fukuoka 819-0395, Japan*
[5] *wolfgang.bruetting@physik.uni-augsburg.de*
**joerg.frischeisen@physik.uni-augsburg.de*

Abstract: Organic light-emitting diodes (OLEDs) usually exhibit a low light outcoupling efficiency because a large fraction of power is lost to surface plasmons (SPs) and waveguide modes. In this paper it is demonstrated that periodic grating structures with almost µm-scale can be used to extract SPs as well as waveguide modes and therefore enhance the outcoupling efficiency in light-emitting thin film structures. The gratings are fabricated by nanoimprint lithography using a commercially available diffraction grating as a mold which is pressed into a polymer resist. The outcoupling of SPs and waveguide modes is detected in fluorescent organic films adjacent to a thin metal layer in angular dependent photoluminescence measurements. Scattering up to 5th-order is observed and the extracted modes are identified by comparison to the SP and waveguide dispersion obtained from optical simulations. In order to demonstrate the low-cost, high quality and large area applicability of grating structures in optoelectronic devices, we also present SP extraction using a grating structure fabricated by a common DVD stamp.

OCIS codes: (050.2770) Gratings; (230.4000) Microstructure fabrication; (240.6680) Surface plasmons; (230.7370) Waveguides; (160.4890) Organic materials; (230.0250) Optoelectronics.

References and links

1. S. Nowy, B. C. Krummacher, J. Frischeisen, N. A. Reinke, and W. Brütting, "Light extraction and optical loss mechanisms in organic light-emitting diodes: Influence of the emitter quantum efficiency," J. Appl. Phys. **104**(12), 123109 (2008).
2. S. Nowy, J. Frischeisen, and W. Brütting, "Simulation based optimization of light-outcoupling in organic light-emitting diodes," Proc. SPIE **7415**, 74151C (2009).
3. L. H. Smith, J. A. E. Wasey, I. D. W. Samuel, and W. L. Barnes, "Light out-coupling efficiencies of organic light-emitting diode structures and the effect of photoluminescence quantum yield," Adv. Funct. Mater. **15**(11), 1839–1844 (2005).
4. S. Reineke, F. Lindner, G. Schwartz, N. Seidler, K. Walzer, B. Lüssem, and K. Leo, "White organic light-emitting diodes with fluorescent tube efficiency," Nature **459**(7244), 234–238 (2009).
5. S. Mladenovski, K. Neyts, D. Pavicic, A. Werner, and C. Rothe, "Exceptionally efficient organic light emitting devices using high refractive index substrates," Opt. Express **17**(9), 7562–7570 (2009).
6. J.-S. Kim, P. K. H. Ho, N. C. Greenham, and R. H. Friend, "Electroluminescence emission pattern of organic light-emitting diodes: Implications for device efficiency calculations," J. Appl. Phys. **88**(2), 1073–1081 (2000).
7. J. M. Ziebarth, and M. D. McGehee, "A theoretical and experimental investigation of light extraction from polymer light-emitting diodes," J. Appl. Phys. **97**(6), 064502 (2005).
8. J. Frischeisen, D. Yokoyama, C. Adachi, and W. Brütting, "Determination of molecular dipole orientation in doped fluorescent organic thin films by photoluminescence measurements," Appl. Phys. Lett. **96**(7), 073302 (2010).

#133491 - $15.00 USD Received 16 Aug 2010; revised 13 Oct 2010; accepted 13 Oct 2010; published 16 Nov 2010

9. D. Yokoyama, A. Sakaguchi, M. Suzuki, and C. Adachi, "Horizontal orientation of linear-shaped organic molecules having bulky substituents in neat and doped vacuum-deposited amorphous films," Org. Electron. **10**(1), 127–137 (2009).
10. J. Frischeisen, D. Yokoyama, A. Endo, C. Adachi, W. Brütting, "Increased light outcoupling efficiency in dye-doped small molecule organic light-emitting diodes with horizontally oriented emitters," (submitted).
11. Y.-J. Lee, S.-H. Kim, J. Huh, G.-H. Kim, Y.-H. Lee, S.-H. Cho, Y.-C. Kim, and Y. R. Do, "A high-extraction-efficiency nanopatterned organic light-emitting diode," Appl. Phys. Lett. **82**(21), 3779–3781 (2003).
12. U. Geyer, J. Hauss, B. Riedel, S. Gleiss, U. Lemmer, and M. Gerken, "Large-scale patterning of indium tin oxide electrodes for guided mode extraction from organic light-emitting diodes," J. Appl. Phys. **104**(9), 093111 (2008).
13. J. M. Ziebarth, A. K. Saafir, S. Fan, and M. D. McGehee, "Extracting light from polymer light-emitting diodes using stamped Bragg gratings," Adv. Funct. Mater. **14**(5), 451–456 (2004).
14. J. M. Lupton, B. J. Matterson, I. D. W. Samuel, M. J. Jory, and W. L. Barnes, "Bragg scattering from periodically microstructured light emitting diodes," Appl. Phys. Lett. **77**(21), 3340–3342 (2000).
15. S. Wedge, I. R. Hooper, I. Sage, and W. L. Barnes, "Light emission through a corrugated metal film: The role of cross-coupled surface plasmon polaritons," Phys. Rev. B **69**(24), 245418 (2004).
16. S. Wedge, A. Giannattasio, and W. L. Barnes, "Surface plasmon-polariton mediated emission of light from top-emitting organic light-emitting diode type structures," Org. Electron. **8**(2-3), 136–147 (2007).
17. S. Wedge, and W. L. Barnes, "Surface plasmon-polariton mediated light emission through thin metal films," Opt. Express **12**(16), 3673–3685 (2004).
18. S. Wedge, J. A. E. Wasey, W. L. Barnes, and I. Sage, "Coupled surface plasmon-polariton mediated photoluminescence from a top-emitting organic light-emitting structure," Appl. Phys. Lett. **85**(2), 182–184 (2004).
19. J. Feng, T. Okamoto, and S. Kawata, "Highly directional emission via coupled surface-plasmon tunneling from electroluminescence in organic light-emitting devices," Appl. Phys. Lett. **87**(24), 241109 (2005).
20. H. Raether, *Surface Plasmons on Smooth and Rough Surfaces and on Gratings* (Springer-Verlag, Berlin, 1988), Chap. 2.
21. S. A. Maier, *Plasmonics: Fundamentals and Applications* (Springer, Berlin, 2007), Chap. 2–3.
22. S. Y. Chou, P. R. Krauss, and P. J. Renstrom, "Imprint lithography with 25-nanometer resolution," Science **272**(5258), 85–87 (1996).
23. S. Harrer, S. Strobel, G. Scarpa, G. Abstreiter, M. Tornow, and P. Lugli, "Room temperature nanoimprint lithography using molds fabricated by molecular beam epitaxy," IEEE Trans. Nanotechnol. **7**(3), 363–370 (2008).
24. S. C. Kitson, W. L. Barnes, and J. R. Sambles, "Surface-plasmon energy gaps and photoluminescence," Phys. Rev. B Condens. Matter **52**(15), 11441–11445 (1995).
25. G. Lévêque, and O. J. F. Martin, "Optimization of finite diffraction gratings for the excitation of surface plasmons," J. Appl. Phys. **100**, 124301 (2006).
26. K. A. Schouhamer Immink, "The digital versatile disc (DVD): System requirements and channel coding," SMPTE J. **105**, 483–489 (1996).
27. J. Moreland, A. Adams, and P. K. Hansma, "Efficiency of light emission from surface plasmons," Phys. Rev. B **25**(4), 2297–2300 (1982).
28. W. H. Koo, S. M. Jeong, F. Araoka, K. Ishikawa, S. Nishimura, T. Toyooka, and H. Takezoe, "Light extraction from organic light-emitting diodes enhanced by spontaneously formed buckles," Nat. Photonics **4**(4), 222–226 (2010).

1. Introduction

In recent years, intensive research and development have been conducted on organic light-emitting diodes (OLEDs) for the realization of high efficiency color displays, backlighting and illumination applications. However, a low light outcoupling efficiency still strongly limits the overall efficiency because only a small fraction of light can leave the multilayer structure due to the large difference in refractive index between air (n = 1.0), glass (n ≈1.5) and organic layers (n ≈1.7 – 2.0). In a typical optimized OLED only about 20% of the light is emitted directly into air and roughly the same amount is coupled to the glass substrate [1]. The remaining power is lost due to the excitation of waveguide modes that propagate inside the organic layers or to surface plasmon polaritons (or simply surface plasmons (SPs)), i.e. guided electromagnetic surface waves traveling along the interface between the organic material and the metallic cathode. Coupling to waveguide modes and SPs causes losses of typically 50% in conventional small molecule based OLEDs [2,3].

In order to extract waveguide modes it was proposed to use high index substrates that have a comparable refractive index as the organic layers. Hence, there is no total internal reflection between organic and glass and no waveguide modes are excited [4,5]. Although this method is very efficient, it increases production costs significantly so that it will probably not be economically advantageous for applications in general lighting.

#133491 - $15.00 USD Received 16 Aug 2010; revised 13 Oct 2010; accepted 13 Oct 2010; published 16 Nov 2010

For the reduction of SP losses, the most apparent way is to simply increase the distance between the emitting molecules and the metallic cathode since the coupling to SPs happens via the optical near field. This has the drawback that the increased total thickness of the organic layers supports more waveguide modes so that often only redistribution from SP to waveguide losses occurs [1]. By contrast, the coupling to SPs can be strongly reduced by using non-isotropic emitters which have their transition dipole moment oriented predominantly horizontally, i.e. parallel to the substrate plane. Since horizontally oriented dipoles dissipate considerably less energy into SPs in comparison with perpendicular ones, the light outcoupling efficiency can be enhanced by a factor of around 1.5. The relevance of emitter orientation has long been known for polymer OLEDs [6,7]. Only recently, this effect has also been discovered for some emitter materials in doped fluorescent organic thin films used in small molecule based OLEDs [8–10]. Despite the huge potential of oriented emitters, it is evident that many emitters that are currently employed in OLEDs show no preferred orientation so that the coupling to SPs cannot be avoided. Consequently, it is necessary to investigate methods in order to transform SPs back into visible light in order to recycle some of the power that is lost to SPs.

A very promising approach for the recovery of surface plasmons is the use of periodic surface structures in order to transform surface plasmons into visible light. One way to achieve this is the integration of a photonic crystal inside the OLED structure [11,12]. Another widely studied method utilizes periodic one- or two-dimensional line gratings. These gratings can be patterned in almost any layer, e.g. into the indium tin oxide anode [12] or into the polymer layer [13]. Alternatively, the grating can be structured into a photoresist in a preprocessing step and the OLED is built on top of this layer [14].

In this study, we follow the latter approach, i.e. fabricating a grating in a preprocessing step into a poly(methyl methacrylate) (PMMA) layer. Usually the grating period used for extraction of surface plasmons lies between 300 nm and 600 nm [11–19]. Here, we demonstrate in a simplified stack under photoluminescence (PL) excitation that even periods above 800 nm, i.e. almost µm-scale, effectively scatter surface plasmons into visible light. In addition to outcoupling of surface plasmons, it is demonstrated that such gratings can be used to scatter and extract waveguide modes that are normally bound inside the organic layers. Optical simulations are used to calculate the dispersion relation of surface plasmons and waveguides which allows the identification of all scattered modes. Finally, we use a grating produced by a common DVD stamp for the extraction of surface plasmons. This demonstrates that the fabrication of periodic scattering structures can be done in a very cost-effective way and with high quality on a large scale.

2. Methodology

Surface plasmon polaritons are electromagnetic surface waves traveling at the interface between a dielectric medium and a metal with maximum intensity at the interface and fields that decay exponentially into both surrounding media [20,21]. Figure 1(a) shows the dispersion relation of light and SPs at a planar interface between an organic layer and a metal.

It is necessary to consider the wave vector component k_x parallel to the substrate plane because surface plasmons are bound to this plane. Therefore, the angular frequency ω is plotted versus the in-plane wave vector k_x. For propagating light this value is defined by $k_x = k_0 \sin\theta$ with θ describing the angle of propagation with respect to the substrate normal and $k_0 = \omega / \mathrm{c}$ being the vacuum wave vector with c the speed of light. All allowed combinations of frequency and in-plane wave vector applicable to freely propagating photons in the air half space are represented as the air light cone in Fig. 1(a). The dispersion of SPs traveling between two semi-infinite layers is described by

$$k_{SP} = k_0 \sqrt{\frac{\varepsilon_m \varepsilon_d}{\varepsilon_m + \varepsilon_d}}, \tag{1}$$

#133491 - $15.00 USD Received 16 Aug 2010; revised 13 Oct 2010; accepted 13 Oct 2010; published 16 Nov 2010

where k_{SP} is the wave vector of surface plasmons, which is per definition in the substrate plane, and ε_m and ε_d are the frequency-dependent relative permittivities of the metal and the dielectric material, respectively.

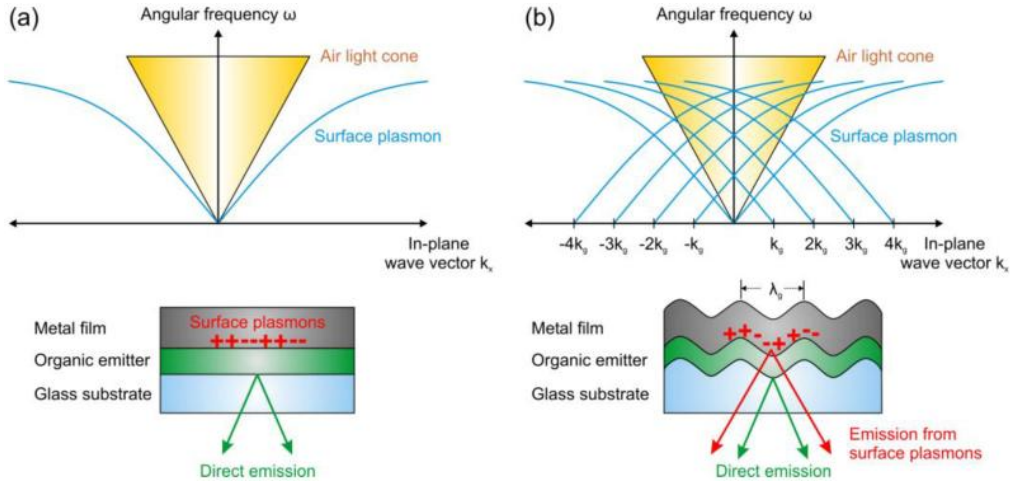

Fig. 1. (a) Schematic dispersion of light and surface plasmons in a sample with planar interfaces. (b) Dispersion in a sample with periodically corrugated interfaces. In the latter case scattering of surface plasmons at the periodic grating may occur which shifts the SP wave vector by a multiple of the grating wave vector.

Apparently, the wave vector of SPs is larger than the in-plane wave vector of light for all frequencies. Thus, no coupling between SPs and light is possible in the case of planar interfaces. Therefore, in a device such as an OLED where an emitting dye molecule excites SPs from the optical near field, power that is coupled to SPs is dissipated as heat and therefore lost.

A very promising method for recovering some of this power is to periodically corrugate the interface, e.g. by a grating with period λ_g, as shown in Fig. 1(b). Such a microstructure allows Bragg scattering of SPs, thus increasing or reducing the wave vector according to the relation

$$\vec{k}'_{SP} = \vec{k}_{SP} \pm m \cdot \vec{k}_g , \qquad (2)$$

where $\vec{k}'_{SP}$ describes the wave vector of the scattered SP mode, $\vec{k}_g$ is the grating wave vector with $\left|\vec{k}_g\right| = 2\pi / \lambda_g$ and m is an integer that defines the order of the scattering process. Depending on the period of the grating and the order of scattering, the SP dispersion can be shifted partly into the light cone as shown in Fig. 1(b). Thus, energy and momentum conservation can be fulfilled for a range of frequencies so that SPs are allowed to couple to far field radiation. Hence, some of the power lost to SPs can be recovered.

All gratings employed in this study are fabricated by nanoimprint lithography [22]. This technique facilitates patterning structures from micro to nano scales with high precision and on a large area. It is a low-cost and high throughput process in comparison to other techniques such as laser interference lithography or electron beam writing [23]. Generally, a hard mold that contains a surface relief structure is pressed into a polymeric resist film that is heated above its glass transition temperature T_g, thereby transferring the grating structure into the polymer; cf. Figure 2(a). Then the temperature is reduced below T_g and the mold is detached. Afterwards, organic and metallic layers are evaporated on the sample in order to create the OLED-like layer structure.

#133491 - $15.00 USD Received 16 Aug 2010; revised 13 Oct 2010; accepted 13 Oct 2010; published 16 Nov 2010

Figure 2(b) shows an overview of all devices used in this study. Devices 1 and 2 are based on the same grating with a period of 833 nm covered with different thicknesses of tris-(8-hydroxyquinoline)aluminum (Alq_3) and capped with silver. In detail, the nanoimprint process was carried out on cleaned microscope slides of approximately 15 × 15 mm^2. The samples were covered with PMMA (Sigma-Aldrich, M_w = 350.000) spin cast from a toluene solution to form a layer of around 450 nm thickness. Just before the imprint was started the samples were heated on a hotplate to 150 °C which is above the glass transition temperature of PMMA (T_g = 105 °C). A pressure of around 50 MPa was applied for several minutes to transfer the microstructure into the PMMA layer. The mold used for the imprint process was a commercially available ruled diffraction grating (Thorlabs, GR13-1205) with a size of 12.7 × 12.7 mm^2 and 1200 lines/mm, corresponding to a grating period of 833 nm. No antisticking layer was used during imprint. The whole process demonstrates the convenience of nanoimprint lithography. Organic and metallic layers were evaporated under a vacuum of around $3 \cdot 10^{-7}$ mbar at a rate of 1.2 and 1.5 Å/s, respectively. The Alq_3 thickness of device 1 was chosen rather low in order to prevent waveguide modes in the organic layer. Therefore, device 1 allows for studying the extraction of surface plasmons exclusively, while device 2 additionally offers a way to study outcoupling of waveguide modes. In addition, a fused silica half cylinder prism is attached to device 1 with index matching liquid in order to extract light propagating inside the glass substrate. Device 3 demonstrates that it is possible to directly imprint the grating structure into the active layer. Therefore, the yellow dye Lumogen Yellow (BASF) was mixed at 5 wt% with PMMA (micro resist technology, ready to use solution with M_w = 75.000) and spin cast onto a glass substrate to form a 180 nm thick layer. The mold used for the imprint process consists of a nickel plate with a standard DVD pattern with 150 nm amplitude and a track pitch of 740 nm. The stamp is covered by a 3 nm titanium layer which acts as an antisticking layer. During the imprint process the sample was heated to 160 °C and then a pressure of 5 MPa was applied for 180 s. Afterwards the sample is cooled down to 80 °C and the mold is released. Finally, 150 nm Ag are evaporated on the sample in the same way as for devices 1 and 2.

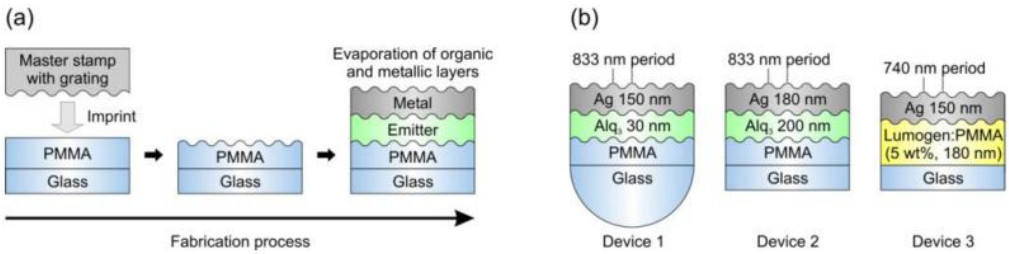

Fig. 2. (a) Illustration of imprint lithography and sample fabrication: The corrugation of the master stamp is transferred to a heated sample consisting of a PMMA layer on glass, producing a replica of the grating. In the last step, organic and metallic layers are evaporated on the PMMA grating. (b) Device overview: Devices 1 and 2 are based on the same grating with 833 nm period but employ a different Alq_3 thickness. In addition, a half cylinder fused silica prism is attached to the backside of device 1. Device 3 uses a 740 nm grating from a DVD stamp which is directly imprinted into the active layer (5 wt% Lumogen Yellow doped into PMMA).

In order to determine the dispersion relation of extracted SPs and waveguides it is necessary to measure the angular dependent emission intensity. For that purpose, the samples are mounted on a computer controlled rotation stage as depicted in Fig. 3. The excitation laser is incident under 45° from the substrate side and rotated together with the sample so that the excitation condition is kept constant during the measurement. The Alq_3 layer in devices 1 and 2 is excited by a 375 nm cw-laser diode. Device 3 is excited by a 473 nm cw-laser diode which fits well to the absorption of Lumogen Yellow. No special encapsulation is required because the Ag layer sufficiently protects the emitting molecules from oxygen and water. The emission is measured from –90° to + 30° in steps of 0.5° through a polarizer because emission from SPs is *p*-polarized. Appropriate longpass filters are employed to protect the

#133491 - $15.00 USD Received 16 Aug 2010; revised 13 Oct 2010; accepted 13 Oct 2010; published 16 Nov 2010

spectrometer from the reflected laser beam. Besides directly emitted light, the excited dye molecules couple to SPs via their optical near field or emit light into waveguides in the case of device 2. SPs and waveguides are scattered at the periodic surface grating so that the dispersion is shifted into the air or glass light cone. Thus, these modes are partly transformed into freely propagating light and can be measured in the experiment.

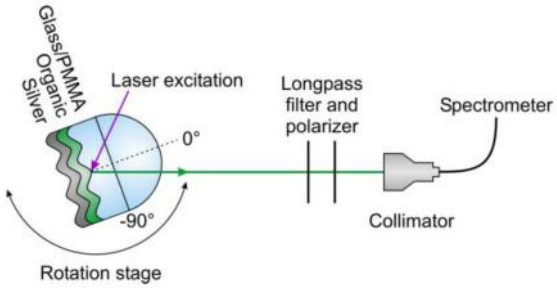

Fig. 3. Experimental setup (top view). A half cylinder fused silica prism is attached to the backside of device 1 whereas devices 2 and 3 are measured without additional outcoupling structure.

3. Optical simulations

In order to identify the extracted modes and the scattering order, the dispersion of SPs and waveguides in all devices was calculated by means of optical simulations. Although Eq. (1) calculates the SP dispersion correctly for semi-infinite layers, it cannot be used for device 1 which incorporates a thin Alq_3 layer with a thickness smaller than the decay length of the evanescent SP field. The optical model used in this study treats the emitting dipoles as damped forced harmonic oscillators embedded in a multilayer structure. A detailed explanation of the method can be found in Ref. 1. We note that simulations are performed for planar layers to obtain the SP and waveguide dispersion relations for the non-corrugated samples. These are afterwards folded back by adding or subtracting multiples of the applied grating wave vectors.

Figure 4(a) shows the total power dissipation in a stack according to device 1. An isotropic dipole orientation is assumed for the simulations and the emitter position is placed in the middle of the Alq_3 layer. Obviously, a large fraction of the power is coupled to SPs because the emitter is located close to the silver layer. There are no waveguides in the organic layer because the Alq_3 layer has a thickness of only 30 nm. In contrast, the thickness of device 2 was chosen so that the emitter couples to a sharp *s*-polarized waveguide mode besides coupling to SPs as shown in Fig. 4(b). It can also be seen that the SP dispersion is located at smaller wave vector values in device 1 compared to device 2. The evanescent field of the surface plasmons in device 1 penetrates into Alq_3 and the adjacent glass layer. The dispersion is thus based on an "effective" refractive index being in between the refractive indices of Alq_3 and glass. Therefore it is located at smaller wave vectors compared to device 2 and the dispersion cannot be calculated by Eq. (1) using the refractive index of bulk Alq_3. By contrast, the SP dispersion of device 2 can be well reproduced by Eq. (1) assuming semi-infinite Ag and Alq_3 layers because the exponentially decaying SP field mainly penetrates into the thick Alq_3 layer. In order to compare the simulation to experiments, the dispersion of SPs as well as the dispersion of the *s*-polarized waveguide mode is extracted from Fig. 4. In addition, the SP dispersion for device 3 is determined from an optical simulation using the same method.

#133491 - $15.00 USD Received 16 Aug 2010; revised 13 Oct 2010; accepted 13 Oct 2010; published 16 Nov 2010

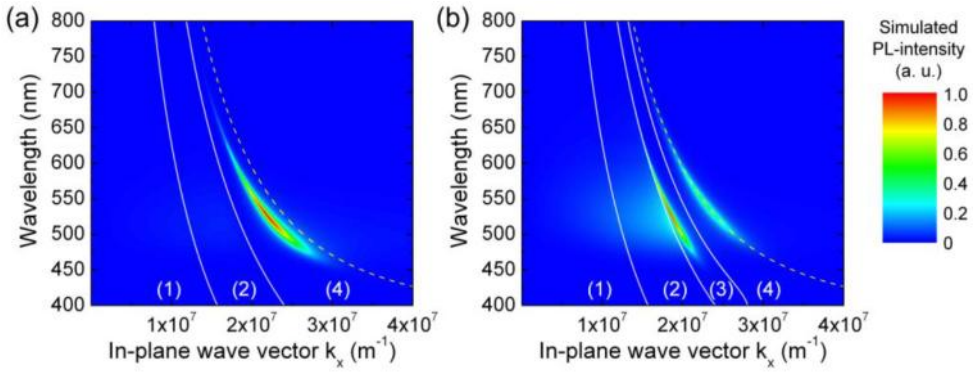

Fig. 4. (a), (b) Simulation of the total dissipated power for devices 1 and 2, respectively, without taking the corrugation into account. The emitter position is assumed to be centered in the Alq_3 layer. Red areas indicate high amount of dissipated power. The solid white lines divide the graph into four regions: emission into air (1), emission into glass substrate (2), waveguide modes (3) and coupling to surface plasmons (4). No waveguide modes exist in device 1 due to the thin Alq_3 layer. The dashed yellow line was calculated using Eq. (1) assuming semi-infinite Ag and Alq_3 layers.

4. Results and discussion

4.1 Characterization of the gratings

Figure 5(a) shows an atomic force microscope (AFM) image of the grating used in devices 1 and 2. The periodic grating has almost no contamination and good long range order.

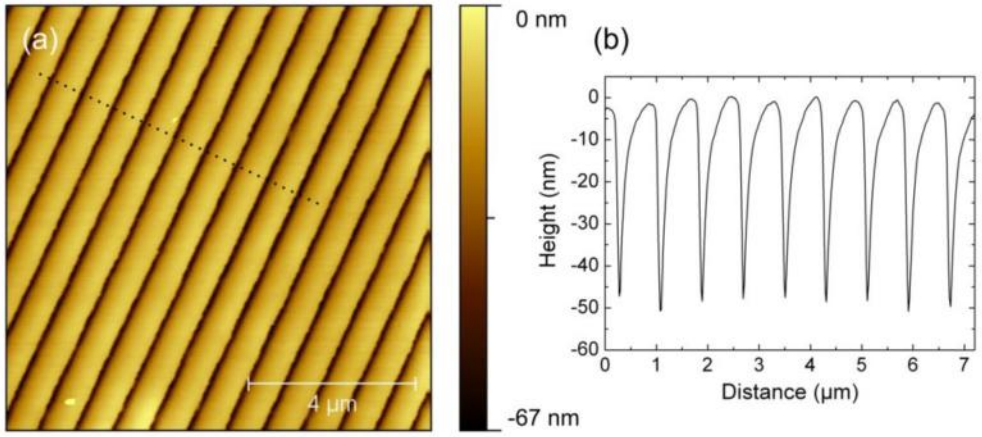

Fig. 5. (a) AFM image of the structure obtained by imprint of a grating with 833 nm period into PMMA as used in devices 1 and 2. (b) Profile at the position indicated by the dotted line in (a).

The profile presented in Fig. 5(b) illustrates that the grating has an amplitude of around 50 nm. The grating period deduced from the profile is approximately 810 nm which is close to the expected value of 833 nm based on the grating manufacturer information.

#133491 - $15.00 USD Received 16 Aug 2010; revised 13 Oct 2010; accepted 13 Oct 2010; published 16 Nov 2010

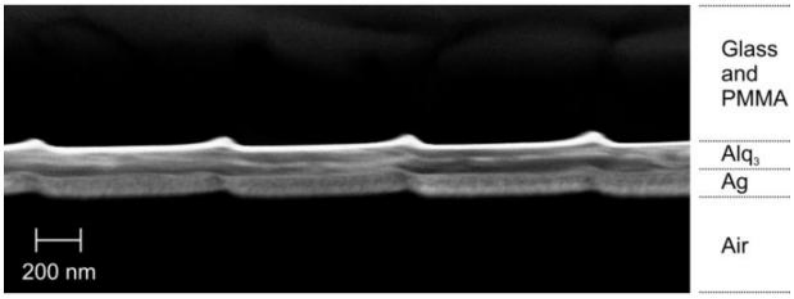

Fig. 6. SEM cross section image of device 2.

The AFM image in Fig. 5 was obtained before evaporation of organic and metallic layers. The structure and amplitude is virtually the same after deposition of Alq_3 and Ag except for a superposition of small Ag islands that are created during the fabrication of the thick Ag layer. In order to demonstrate that the grating is transferred from the structured PMMA layer to Alq_3 and Ag, a scanning electron microscope (SEM) image of a cleaved edge of device 2 is presented in Fig. 6. It can be clearly seen that all deposited layers above PMMA adopt the periodic structure. In addition, the periodicity of the grating can also be deduced from Fig. 6. An average grating period of around 840 nm is obtained which again agrees well with the expected value.

4.2 Extraction of surface plasmons

The measured *p*-polarized emission of device 1 with a 30 nm Alq_3 layer is presented in Fig. 7. Besides a background of directly emitted light there are several strongly dispersive features which result from scattered SPs that are transformed into visible light. A half cylinder prism is attached to device 1 so that not only the scattered modes within the air light cone but also those within the glass light cone can be extracted. Several band gaps are observed at crossing points of two SP dispersions where diffracted waves traveling in opposite direction interact. The width and location of the band gap depends on the grating shape and period [24,25]. The lines in Fig. 7 were obtained from the simulated SP dispersion shown in Fig. 4(a) and shifted by a multiple of the grating wave vector with a period of 833 nm according to Eq. (2). The general agreement between the simulated and measured angular position of the scattered SPs is very good. Slight deviations are probably caused by a not perfectly perpendicular alignment of the grating or by small errors concerning the period of the grating or the optical constants and thicknesses used in the simulation. It should be noted that Eq. (2) only gives information about the location of the scattered SPs whereas the intensity of the different orders may also depend on the actual geometry of the grating.

It is noteworthy that a strong SP emission is obtained although the period of the grating is almost on a µm-scale. Usually smaller periods are used so that first-order scattered SPs lie within the air light cone. Here the larger period is compensated by higher order scattering. In fact, even 5th-order scattering can still be detected and identified in Fig. 7. Therefore, we anticipate that even a grating with such a large period and thus easier and cheaper fabrication should be considered to be used as outcoupling enhancement in OLEDs. In addition, the occurrence of many diffracted modes may even offer an improvement concerning the color shift of the angular dispersive emission.

A rough estimation of the extraction efficiency can be achieved from an analysis at fixed wavelength and the comparison of directly emitted light versus extracted SPs. For that purpose, Fig. 8(a) and (b) show cross sections of Fig. 7 at 575 nm and 625 nm, respectively. The wavelengths are chosen so that there is almost no SP emission at zero degree and hence the intensity at this point can be attributed to directly emitted light. The results differ inasmuch as Fig. 8(a) shows a cross section close to the photonic band gap where two diffracted waves having almost the same emission angle overlap, while Fig. 8(b) is further

#133491 - $15.00 USD Received 16 Aug 2010; revised 13 Oct 2010; accepted 13 Oct 2010; published 16 Nov 2010

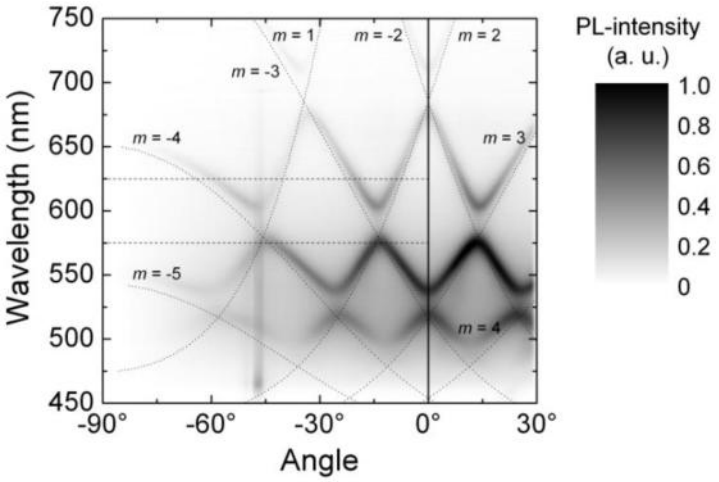

Fig. 7. Measurement of the *p*-polarized emission of device 1. The dotted lines represent the dispersion of surface plasmons obtained from Fig. 4(a) shifted by a multiple *m* of the wave vector of an 833 nm grating. Negative values of *m* denote scattering of surface plasmons traveling in the positive k_x-direction and vice versa. The higher emission around –47° results from reflections of the incident laser beam. The two horizontal dashed lines indicate the position of the cross sections shown in Fig. 8.

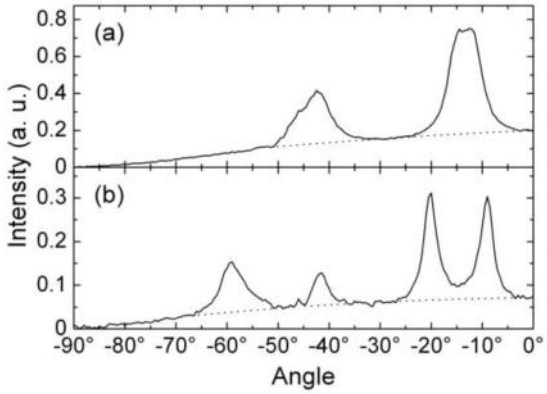

Fig. 8. (a), (b) Cross section of Fig. 7 at a wavelength of 575 nm and 625 nm, respectively. The dotted lines approximately indicate the contribution of directly emitted light. The increased intensity around –47° due to the reflected laser has been manually subtracted.

away from the band gap, hence there are four distinct peaks observable. By integrating over the cross sections it is found that the emission arising from extracted SPs amounts to around 70% of the fraction of directly emitted *p*-polarized light. It should be noted that this value does not correspond to the extraction efficiency of SPs because it is not known to which extent the emitting molecules couple to SPs and to direct emission, even though the coupling to SPs is expected to be the dominant loss channel. For an accurate determination of the extraction efficiency an optical simulation that takes structured interfaces with different periods and amplitudes into account might be favorable. It should be noted that a detailed investigation of the efficiency must also consider the fact that the incident laser can be scattered by the grating which may change the excitation conditions considerably.

From the position of the peaks in Fig. 8(b) it is also possible to derive the grating period. By comparing the cross section to Fig. 7 it is found that the peaks at –9° and –41.5° originate from SPs propagating in the same direction but differing in the order of scattering by one. The same applies to the peaks at –20° and –59°. The corresponding in-plane wave vector values

#133491 - $15.00 USD Received 16 Aug 2010; revised 13 Oct 2010; accepted 13 Oct 2010; published 16 Nov 2010

can be calculated using $k_x = (2\pi \cdot \mathrm{n}/625\mathrm{nm}) \cdot \sin\theta$ with the refractive index of fused silica of n ≈1.457 at this wavelength. The difference in the values for the in-plane wave vector between two of these peaks is approximately $7.48 \cdot 10^6$ m^{-1} which corresponds to a grating period of around 840 nm, i.e. close to the value expected from the manufacturer information.

4.3 Extraction of surface plasmons and waveguide modes

Device 2 features a thicker Alq_3 layer of around 200 nm so that the emitting molecules can couple to a waveguide mode besides the excitation of SPs. From the *p*-polarized emission shown in Fig. 9 it is obvious that the measurement basically looks similar to the emission of device 1, although the SP dispersion is slightly different as was discussed in the results of the optical simulation in Sec. 3. Using the SP dispersion obtained from Fig. 4(b), there is good agreement between measured and simulated angular position.

The main difference between device 1 and 2 is that no outcoupling prism is attached during the measurement of device 2. Therefore only the modes scattered into the air light cone are accessible by the measurement and thus less scattered SP features are observable in Fig. 9 compared to Fig. 7. Nevertheless, this demonstrates that it is not necessarily required to attach outcoupling structures in order to extract SPs which are scattered at periodic gratings.

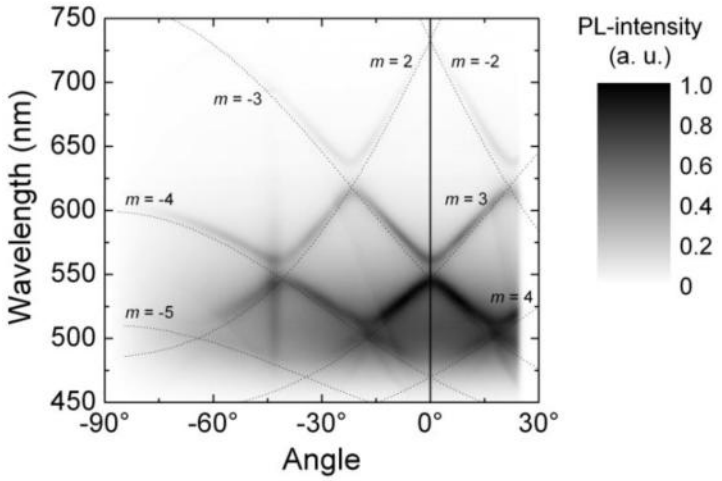

Fig. 9. Measured *p*-polarized emission of device 2. The lines are obtained from the dispersion of surface plasmons shown in Fig. 4(b) shifted by a multiple of the wave vector of an 833 nm grating.

The measured *s*-polarized emission displayed in Fig. 10 shows that a sharp *s*-polarized waveguide mode exists in the 200 nm thick Alq_3 layer as expected from the optical simulation. By extracting the dispersion of this waveguide mode from Fig. 4(b) and using Eq. (2) also for scattering of waveguides, very good agreement between the measured and simulated angular position is obtained. Scattering up to 4th-order is observed in the measurement.

It is noteworthy that the maximum absolute intensity is more than 10 times larger for the *s*-polarized measurement in comparison to the measured *p*-polarized emission. The main reason for this is that coupling to the *s*-polarized waveguide mode occurs through the whole 200 nm thick Alq_3 layer while SPs are mainly excited from molecules close to the silver. Furthermore, since the laser is incident from the glass side, a large fraction of the laser intensity is already absorbed before molecules close to the silver are excited. It should be noted that also a very weak *p*-polarized waveguide mode emerges at short wavelengths in the measurement and simulation of device 2. However, this feature is hardly visible and the simulated dispersion lines have thus been omitted in Fig. 9 for reasons of clarity.

#133491 - $15.00 USD Received 16 Aug 2010; revised 13 Oct 2010; accepted 13 Oct 2010; published 16 Nov 2010

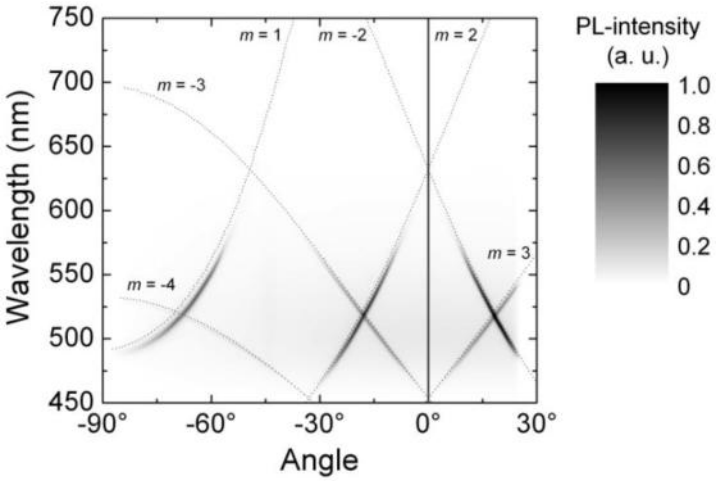

Fig. 10. Measured *s*-polarized emission of device 2. The lines are obtained from the dispersion of the waveguide mode shown in Fig. 4(b) shifted by a multiple of the wave vector of an 833 nm grating.

4.4 Outcoupling enhancement with DVD gratings

The microstructured grating used in device 3 is based on a common DVD stamp as described previously in Section 2. Figure 11(a) presents an AFM image of the sample after the imprint process which shows the individual DVD tracks next to each other. Although each track is discontinuous, there is a periodic spacing between the tracks. This distance is known as track pitch and has a value of 740 nm in a DVD [26]. From the profile shown in Fig. 11(b) an average period of around 730 nm is obtained which fits quite well to the track pitch.

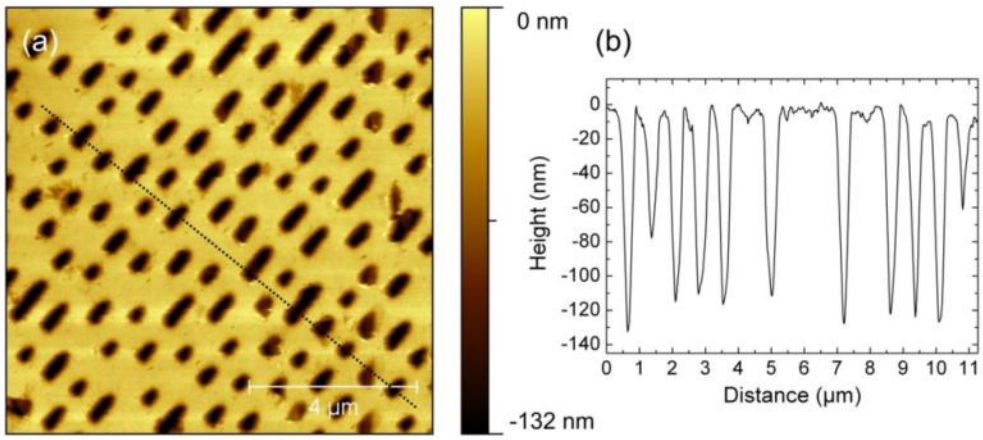

Fig. 11. (a) AFM image after imprinting a DVD stamp into the Lumogen:PMMA layer used in device 3. The DVD track runs diagonally from the top right to the bottom left corner. (b) Profile at the position indicated by the dotted line in (a).

The amplitude is found to have a value of up to 130 nm. The most efficient coupling between SPs and light occurs for a grating amplitude of some tens of nanometers [25,27]. Therefore, we spin cast poly(3,4-ethylenedioxythiophene)/poly(styrenesulfonate) (PEDOT/PSS, AI 4083, H.C. Starck) onto the sample. This polymer material is water based so that PMMA is not dissolved again. Although the wetting of PEDOT/PSS is very bad on PMMA, the surface was smoothed and the holes were partially filled so that the amplitude was slightly reduced.

#133491 - $15.00 USD Received 16 Aug 2010; revised 13 Oct 2010; accepted 13 Oct 2010; published 16 Nov 2010

The measured *p*-polarized emission of device 3 is displayed in Fig. 12. Although the amplitude still is not optimal, several dispersive SP features are distinguishable. This is remarkable considering that the individual grating lines are discontinuous and irregular. However, the periodic line pitch of the DVD structure appears to be sufficient in order to scatter SPs and extract them as visible light.

The theoretical SP dispersion is again calculated in a similar way as presented for devices 1 and 2. Here, the SPs are traveling along the interface between Ag and PMMA at smaller wave vectors compared to both other devices, because PMMA has a smaller refractive index than Alq_3. It should be noted that no waveguide modes exist in this stack because there is no total internal reflection between PMMA and glass since both materials have a quite similar refractive index. Shifting the calculated SP dispersion by a multiple of the grating wave vector of a 740 nm grating gives excellent agreement with the measured result as shown by the lines in Fig. 12.

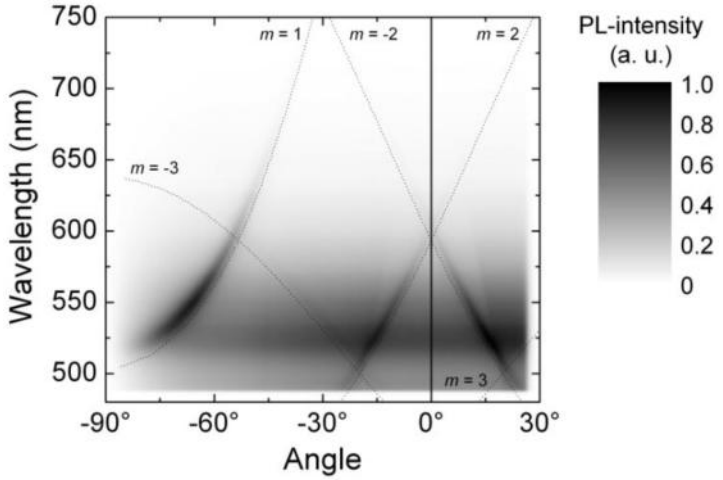

Fig. 12. Measurement of the *p*-polarized emission of device 3. The lines represent the SP dispersion obtained from a simulation of device 3 shifted by a multiple of the wave vector of a 740 nm grating which corresponds to the track pitch of a DVD.

Certainly, a continuous grating with optimized amplitude would show a much more efficient SP extraction. However, the fact that the basic principle works even with a DVD structure promises that SPs can be extracted even if some defects or irregularities occur during the fabrication process. Further improvement concerning the color shift of the angular dispersive emission could be obtained by using a quasi-periodic structure with broad distribution and directional randomness as reported by Koo *et al.* who employed buckles which were spontaneously formed during cooling of a thin aluminum layer [28]. It should be noted that the fabrication of quasi-periodic layers is also compatible with the presented nanoimprint technique if an appropriate mold is used.

All in all, using a DVD stamp for the extraction of SPs demonstrates that it is indeed possible to fabricate gratings for optoelectronic devices with excellent quality on a large area at remarkably low cost, keeping in mind the quality, size and costs of commercially available DVD molds.

5. Conclusions

In summary, we have studied the light outcoupling enhancement by extraction of surface plasmons and waveguide modes in OLED-like devices using nanoimprinted grating structures with almost µm-scale period. Despite the comparatively large period, extraction of SPs and waveguides by scattering up to 5th-order could be detected. The determined angular position of the extracted modes agrees very well with the dispersion relation of SPs and waveguides

#133491 - $15.00 USD Received 16 Aug 2010; revised 13 Oct 2010; accepted 13 Oct 2010; published 16 Nov 2010

obtained from optical simulations and shifted by a multiple of the grating wave vector. This demonstrates that it is not always necessary to use gratings with a period below 500 nm which are usually more expensive and complex in fabrication, although the employment of such gratings could result in an increased extraction efficiency due to first order scattering. On the other hand, an advantage of gratings with larger periods is the occurrence of more diffracted modes, hence the emission has less color shift. Strictly speaking, it is preferable to further investigate and compare different grating periods and balance their extraction efficiency against manufacturing costs. It might also be interesting to study the influence of other metals with higher absorption or additional ITO layers with rather high refractive index. Clearly, the effect of grating structures in real OLED devices under electroluminescence will also be an important topic for future work. In order to demonstrate the low-cost, high quality and large area applicability of grating structures in optoelectronic devices, we verified SP extraction by means of a grating structure produced with a common DVD stamp. The extraction efficiency can be further enhanced by optimizing the shape and amplitude of the grating. Finally, it should be noted that such grating structures can also be employed in other organic optoelectronic devices such as organic lasers that use a distributed feedback structure.

Acknowledgments

The authors acknowledge financial support by the Elite Network of Bavaria through the international graduate school "Materials Science of Complex Interfaces", by the Japan Society for the Promotion of Science (JSPS), by a Grant-in-Aid for the Global COE Program "Science for Future Molecular Systems" from the Ministry of Education, Culture, Sports, Science and Technology of Japan, by the Funding Program for World-Leading Innovative R&D on Science and Technology (FIRST), by the IAS, Focus group "Nanoimprint and Nanotransfer" and by the German Federal Ministry of Education and Research (BMBF) under contract FKZ 13N10474 (TOPAS 2012). We are most thankful to Rosemarie Heilmann for experimental support in the lab.

#133491 - $15.00 USD Received 16 Aug 2010; revised 13 Oct 2010; accepted 13 Oct 2010; published 16 Nov 2010